

NRGA: Gravitational Approach for Non-Rigid Point Set Registration

Sk Aziz Ali

Sk_Aziz.Ali@dfki.de

Vladislav Golyanik

Vladislav.Golyanik@dfki.de

Didier Stricker

Didier.Stricker@dfki.de

University of Kaiserslautern, Germany
German Research Center for Artificial Intelligence (DFKI GmbH)

Abstract

Recovery of correspondences between point sets which differ by some non-rigid transformation is an ill-posed problem. Many existing methods underperform on noisy or corrupted input data. In this study, a novel physics-based approach – Non-Rigid Gravitational Approach (NRGA) – for non-rigid point set registration is introduced which is robust to the mentioned artifacts. Thereafter, a distributed N-body simulation and iterative Procrustes alignment non-rigidly transform and register the template point set. Furthermore, in the force field evolution, per-point Gaussian curvature serves as a shape matching descriptor whereas the displacement fields are regularized by coherent collective motion. The optimal alignment is referred to as the state of minimum gravitational potential energy between the point sets. A thorough experimental evaluation and comparison are provided with widely used state-of-the-art methods on 2D and 3D datasets. Experiments show NRGA’s robustness against uniform outliers and missing data.

1. Introduction

Point set registration is a fundamental and challenging problem in computer vision. The appearances and characteristics of the input point sets can be different (*e.g.*, density, the underlying structure they represent, origin, *etc.*), and the objective is to recover the correspondences and displacement fields which reasonably – according to some application criteria – transforms one point set to other. A point set which has fixed position and remains unchanged is called *reference*, and the other one which is being transformed is called *template*. The non-rigid point set registration problem is considered similar to the other classes of pattern matching problems like image registration (using color cues and other image-based descriptors for 2D and volume images)[12, 19], or shape registration (using points, normals, faces and other shape features for different types of deformation like large, articulated, locally isomet-

ric, conformal *etc.*) [33, 36]. The majority of the mentioned variant classes solve the registration problem by defining a distance error metric to optimize either for the deformation or the displacement field. The deformation field can be an implicit function of transformation parameters which are often regularized in conjunction.

Any non-rigid point set registration method finds difficulty to tackle noisy or corrupted data (such as missing chunks and clustered outliers) and to perform good when input data are misaligned. Most widely-used instances are descendants of iterative closest points (ICP) techniques [2]. The main idea of ICP-like methods consists in alternating between nearest neighbor search and transformation updates, over and over until no changes are occurring.

Another prominent class of methods employs probabilistic approaches (*e.g.*, expectation-maximization) which explain observed reference data by a deformable template [26, 7]. These methods inherit strengths and disadvantages of the underlying unsupervised learning techniques, and many approaches are sensitive to disturbing effects. As noticed by Jian and Vemuri [20] more than a decade ago, there is no clear winner among probabilistic approaches, and this is still the case in the present. This aspect motivates us to look into the alternative directions.

The physics-based class is a new class of point set registration methods. One method employs Schrödinger transformation for non-rigid alignment [8], and the other one employs modified *N*-body simulation for rigid matching [15]. Both methods were shown to outperform representatives of other classes — in many cases by a noticeable margin — which suggests that have a high potential for further improvements. In addition, non-rigid registration methods often compromise with either correspondence accuracy or geometric consistency during data fitting. Some deformable registration methods [29, 3] mainly address the geometric smoothness factor, whereas, distance based non-rigid transformation methods [1, 20] primarily prioritize correspondence accuracy. A registration method which balances both is desirable.

We propose a non-rigid point set registration method

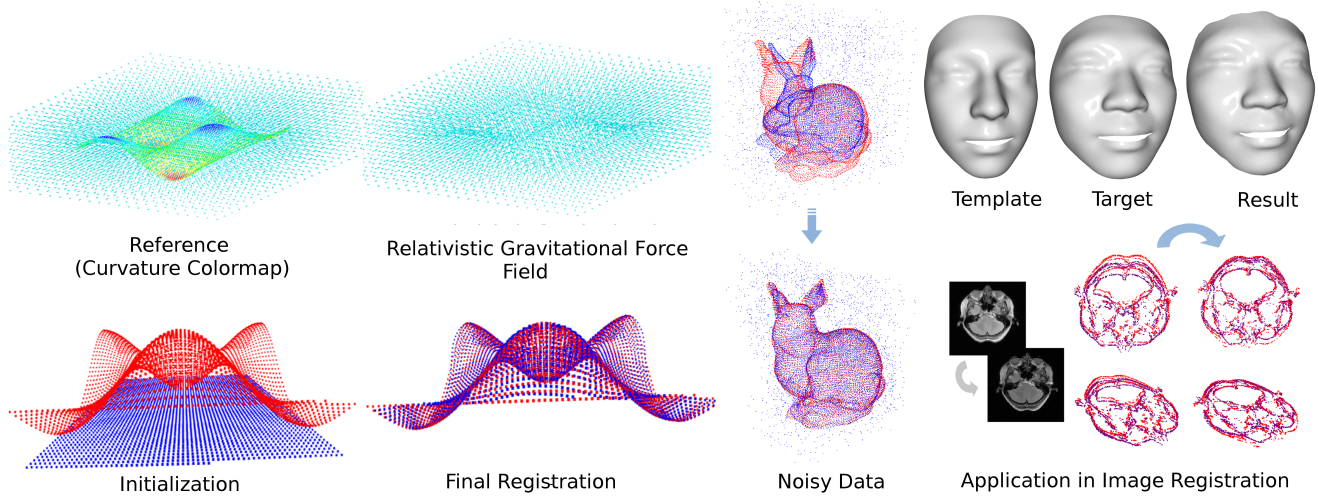


Figure 1. The NRGA method uses the law of universal gravitation for non-rigid alignment of point sets. On the left, the *Cosine Surface* dataset $f(x, y) = \cos(x) \sin(y)$ induces *relativistic gravitational force* field to attract the plane $f(x, y) = -1$, where $x, y \in [-\pi, \pi]$. On the right, various registration results are demonstrated, i.e., noisy bunny [35] data alignment, conformal registration between human faces of different expressions (from [4] on BU-3DFE [41]), and image registration between computer tomography of a human brain [38].

which is based on simulation of gravitational interactions between points. Speaking in physical analogies, we think of the points as particles with masses interacting inside an isolated non-empty space according to the universal law of gravitation. We call this method Non-Rigid Gravitational Approach (NRGA). We see NRGA as the first to generalize the principles proposed in [15] to the non-rigid case. The solution-space is much larger for non-rigid registration. To reduce it, we apply coarse-to-fine zonal interaction, preservation of relative point position during motion and regularization of the displacement fields. Fig. 1 illustrates how the reference induces gravitational force fields near it. The template deforms until a state of minimum gravitational potential energy (GPE) is obtained between them. As opposed to single rigid transformation constraint on the whole template in [15], in NRGA every single template point undergoes a coherent Procrustes transformation, approximating local transformation manifold around them (Secs. 4.2 and 4.3).

In total, there are several **contributions** in this work — i) We present NRGA as the first method for non-rigid point set registration in the gravitational class (Sec. 4). From the point of algorithmic novelty, NRGA lets every template point choose their own interaction zone from the reference point cloud. It splits the template and the reference into as many numbers of overlapping subsets as of the numbers of template points. ii) Then, a series of locally multiply-linked N -body problems are solved where the gravitational force function is parameterized by the Gaussian curvature [10] (Sec. 4.1 and 4.2) of reference points. This generalizes the gravitational force in a curved space-time and gives a strong hypothesis to match point sets. The main idea of

having such overlapping zones is to obtain many unconstrained (suboptimal) motion update hypotheses and regularize them finally for individual displacements. iii) *Coherent Collective Motion* (CCM) operator, which is often used in the simulation of biological species [37], is used as motion and transformation regularizer in our method (Sec. 4.3).

Finally, we evaluate the new approach (Sec. 5) qualitatively and quantitatively on synthetic and real-world datasets. In the experiments, NRGA exhibits robustness against missing data and uniform noise, when compared to widely used state-of-the-art methods.

2. Related Work

In this section, we provide a concise overview of modern non-rigid point set registration methods and position the proposed NRGA among them. Though the body of literature on non-rigid point set registration is versatile, current approaches can be classified into few categories.

Coarsely, the primary classes either involve nearest-neighbor search step [2, 30] (variants of ICP), employ various probabilistic principles for unsupervised learning of optimal transformation fields [20, 23], or are physics-based schemes which adopt or simulate natural and physical phenomena [22, 8].

Each category can be further refined through multiple subcategories differentiating between used optimization techniques (deterministic annealing scheme in [6], expectation-maximization [23]), acceleration techniques (spherical triangle constraint for nearest neighbor search in ICP [17]), types of probabilistic models and distributions (Gaussian mixture model of GMMReg [20] versus

Student's-t mixture model [42]), types of borrowed physical laws (Schrödinger distance transform [8]) or types of displacement field regularizers (a thin-plate spline in [6] or variational regularizer of motion coherence in [26]). Moreover, auxiliary classifications distinguish between two point set (hereto belongs the majority of the approaches) and multi-set registration [31], whether methods allow to embed priors matches (akin to ICP methods) or require some additional information aside from 3D coordinates [1, 14]¹.

With only a few representatives in both rigid and non-rigid domains [15, 8], the class of physics-based methods is the least explored in point set registration. Many physical phenomena involve an interaction of elements and allow a quantitative description of the system's state based on the configuration of their elements (gravitational or electrostatic potential energy, quantum state). Another example is the visual system of stereopsis-capable biological species which is uninterruptedly solving the registration task of vector-valued images (signals arising on the retina) [27].

Though the curvature was used in shape and image registration before [12, 13, 32, 34, 33], its application in point set registration is not straightforward. One reason is that for an arbitrary point set, the curvature is not everywhere defined. Due to the synergy of direct curvature retrieval on a point set and post-Newtonian mechanics, NRGA allows to overcome this limitation and define curvature in every point of space, irrespective whether the point set represents a surface or a volumetric structure, perhaps a non-uniformly sampled one and containing outliers. This is the crucial property not found in other point set registration methods. At the same time, many such existing methods chose either global motion coherency [39, 26] or local shape signatures [24] to preserve the overall topology. In contrast, the CCM regularizer in NRGA can be viewed as a locally-aware global topology preservation operator.

Our method is related to GA [15]. We adopt the idea of N -body simulations and generalize it to the non-rigid case. Instead of recovering one single global rigid transformation, we recover per-point displacements. To this end, in NRGA every template's point has its own transformation.

3. N-Body Simulation

In the classical N -body problem, N celestial bodies define their kinematic trajectories by interacting with each other through a conservative gravitational force field [9]. Every celestial body possess a mass, and the interactions are governed by the Newton's law of universal gravitation. The gravitational forces between the celestial bodies, often in large scale system, accounts for the change in GPE.

¹though, with too many additional inputs, the class of methods might change; for instance, shape registration considers alignment of watertight meshes, *i.e.*, point sets with known triangulation, normals, *etc.* and constitutes a separate branch of research.

GPE is defined as the work done by the gravitational force to displace the particle from one to another position. Most frequently, the masses are assumed to be concentrated in an infinitely small volume of space and inter-collisions are not taken into account (no merging, splitting and re-distribution of masses are allowed). Thus, if a system consists of a plenum space and a set of particles $i \in \{1, \dots, N\}$ with masses m_i , positions \mathbf{r}_i , then the total force acting on i^{th} particle \mathbf{F}_i is equal to the sum of the negative gradient of the gravitational potential ϕ_i^a and, if exists, some external potential ϕ_i^{ext} (*i.e.*, in other terms, as the sum of the force components \mathbf{F}_i^a and $\mathbf{F}_i^{\text{ext}}$):

$$\mathbf{F}_i = -\nabla(\phi_i^a) - \nabla(\phi_i^{\text{ext}}). \quad (1)$$

The former force component \mathbf{F}_i^a for the discrete particle system

$$\mathbf{F}_i^a = -Gm_i \sum_{j=1, j \neq i}^N \frac{m_j (\mathbf{r}_i - \mathbf{r}_j)}{\left(\|\mathbf{r}_i - \mathbf{r}_j\|^2 + \epsilon^2\right)^{\frac{3}{2}}} \quad (2)$$

is used to numerically approximate particle's position over time, where G is the gravitational constant, $\|\cdot\|$ denotes the ℓ_2 norm, and ϵ is a regularizer of near-field interactions called softening radius; $j \in \{1, \dots, N\}$, $j \neq i$ indexes $N - 1$ particles exerting gravitational force of attraction on i^{th} particle. Per particle acceleration is updated by the Newton's Second Law of motion:

$$\ddot{\mathbf{r}}_i = \frac{\mathbf{F}_i^a}{m_i}, \quad (3)$$

and \mathbf{r}_i is obtained by the double integration of acceleration $\ddot{\mathbf{r}}_i$ over time.

With the advent of the Einstein's general relativity (GR) [11], the perspective to the interaction between masses has changed. According to modern GR, celestial masses bend the space-time continuum. The bending strength changes space-time curvature which is expanded into a separate dimension. The celestial masses placed in the curved space-time do not move along straight lines but rather curved lines. The latter phenomenon causes the effect known in Newtonian mechanics as gravitational force, whereas in GR, gravitational force does not exist. Thus, in presence of mass, the space-time is a non-flat four-dimensional manifold \mathbb{M}^4 (Minkowski space). In GR, space-time curvature depends on the mass and energy distribution in space, the speed of light and G [40]. On the other hand, space-time curvature influences G .

Even though gravitational force in GR is replaced by the curvature of the 4D space-time, we use the notion of *relativistic gravitational force* (RGF), *i.e.*, a gravitational force parameterized by the Gaussian curvature of the force inducing particles (Sec. 4).

Eventually, the N -body problem was extended to the case of relativistic motion. Considering NRGA, we are especially interested in the simulation in a space with a constant Gaussian curvature [10] so that RGF takes the form:

$$\mathbf{F}_i^a = -Gm_i \sum_{j=1, j \neq i}^N \frac{m_j \left(\mathbf{r}_i \left(1 - \frac{\kappa \mathbf{r}_{ij}^2}{2} \right) - \mathbf{r}_j \right)}{(\|\mathbf{r}_i - \mathbf{r}_j\|^2 + \epsilon^2)^{\frac{3}{2}} \left(1 - \frac{\kappa \mathbf{r}_{ij}^2}{4} \right)^{\frac{3}{2}}}, \quad (4)$$

with $\mathbf{r}_{ij} = \|\mathbf{r}_i - \mathbf{r}_j\|$ and κ denoting constant Gaussian curvature of the space. Similar to the classical case, acceleration $\ddot{\mathbf{r}}_i$ is computed by Eq. (3) and (4), and new \mathbf{r}_i is updated as double integrals of $\ddot{\mathbf{r}}_i$ w.r.t. time.

4. Non-Rigid Gravitational Approach

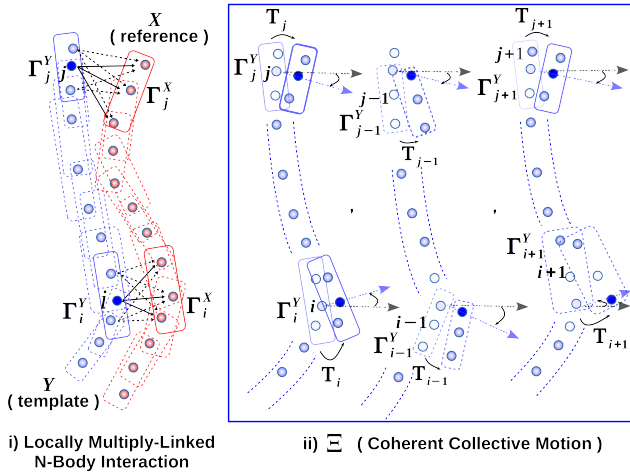


Figure 2. NRGA is comprised of two integral steps: i) applying locally multiply-linked N -body interactions between all the corresponding regions. This local gravitational interactions estimate the next point positions. i^{th} and j^{th} points select few nearest points from Y and X to represent regions Γ_i^Y and Γ_j^X bounded by solid blue and red colour lines from Y and X respectively. Rigid transformation parameters T_i are obtained for all regions with Procrustes alignment between consecutive states. ii) applying coherent collective motion regularizer on final position update (as a consensus filter on all T_i).

Given two point sets, a *reference* or target $\mathbf{X}_{N \times D} = (\mathbf{X}_1, \dots, \mathbf{X}_N)^T$, and a *template* or source $\mathbf{Y}_{M \times D} = (\mathbf{Y}_1, \dots, \mathbf{Y}_M)^T$ with N and M number of D dimensional points respectively, the objective is to find a transformation mapping $\mathcal{T} : \mathbb{R}^D \rightarrow \mathbb{R}^D$ which minimizes a distance error function between two sets. In NRGA, this error function is the total GPE of \mathbf{Y} w.r.t \mathbf{X} which can be expressed as a sum of weighted inverse values of the Euclidean distances:

$$\phi_a = \arg \min_{\mathbf{T}} \sum_{i=1}^M \sum_{j=1}^{|\mathcal{N}(i)|} \omega_{ij} (d(\mathcal{T}(\mathbf{Y}_i, \mathbf{T}_i) - \mathbf{X}_j))^{-1}, \quad (5)$$

where $\omega_{ij} = -Gm_i m_j$ denotes the weight of i^{th} minimum GPE amongst its nearest neighbors $\mathcal{N}(i)$, and $d(\mathbf{Y}_i, \mathbf{X}_j) = \|\mathbf{Y}_i - \mathbf{X}_j\| + \epsilon$ is the numerically stabilized Euclidean distance. The transformation map $\mathcal{T}(\mathbf{Y}, \mathbf{T})$ registers \mathbf{Y} to \mathbf{X} using the set of optimal transformation tuples $\mathbf{T} = \{\mathbf{T}_1, \dots, \mathbf{T}_M\}$. We employ N -body problem in curved space (Eq. (4)) as an inverse problem toolbox to iteratively solve for the optimal transformation parameters \mathbf{T}_i and attain the minimum value of energy function in Eq. (5). In this process, the points represent particles with individual masses; the process is collision-less. The overall registration process includes three steps —

First, we build k-d trees on \mathbf{X} and \mathbf{Y} separately. Since \mathbf{X} is always static and remains unchanged, we keep the k-d tree on \mathbf{X} same and rebuild the tree on \mathbf{Y} in every iteration as it deforms.

Second, in every iteration, each \mathbf{Y}_i selects a number of nearest neighbors (see Sec. 4.2) from \mathbf{X} and \mathbf{Y} to define a zone of influence Γ_i^X and Γ_i^Y respectively. It reduces the solution space for every \mathbf{Y}_i . We use the k-d trees to obtain the nearest neighbors. For every \mathbf{Y}_i , Γ_i^X attracts the corresponding zone Γ_i^Y , employing N -body problem parameterized by the Gaussian curvature of \mathbf{X} . This is a locally multiply-linked point-to-point interaction. Once the force fields are computed, we independently update the *template* point positions in Γ_i^Y . From the previous and current state of Γ_i^Y , unconstrained transformation tuple \mathbf{T}_i is obtained using Procrustes alignment [21]. Serially, we estimate \mathbf{T} for all Γ_i^Y , where $i \in \{1, \dots, M\}$. Every tuple \mathbf{T}_i is a transformation representative for the group of points in Γ_i^Y . Conversely, a template point \mathbf{Y}_i can have multiple transformation representatives as the adjacent regions overlap. In every iteration, only the velocity of representative points from each group are updated.

Third, we use coherent collective motion (CCM) operator Ξ to consolidate multiple unconstrained transformation fields and velocities for every \mathbf{Y}_i into an optimal update. The locally optimal solution is achieved when GPE of the system reaches its minimum. The two integral steps of NRGA are shown in Fig. 2.

4.1. Modified N -body problem

Several additional assumptions are made in NRGA to adopt and fit the relativistic N -body problem toolbox compared to Sec. 3. *First*, only \mathbf{X} induces gravitational field and remains fixed (see Fig. 1). We compute the force values on demand, whereas the curvature of \mathbf{X} is precomputed following [28]. *Second*, we avoid gravitational interactions between the particles from the same set (e.g., \mathbf{Y}), otherwise the template and reference would deform at rest and topology will be lost. *Third*, the external potential energy in Eq. (1), is considered here as a dissipative loss. This consideration is natural when the space is non-empty. Hence, we

add an external drain force \mathbf{F}_i^{ext} to \mathbf{F}_i^a as a small fraction η of its velocity acting in the opposite direction:

$$\mathbf{F}_i^{ext} = -\eta \dot{\mathbf{r}}_i. \quad (6)$$

As a result, a part of the system's kinetic energy is dissipated in every iteration.

4.2. Locally Multiply-Linked N -Body Problem

NRGA is a locally multiply-linked method which iteratively registers \mathbf{Y} to \mathbf{X} . The groups of nearest neighbor multi-sets from \mathbf{Y} and \mathbf{X} , further metasets of point indices, are denoted by $\mathcal{R}_{\mathbf{Y}} \equiv \{\Gamma_1^{\mathbf{Y}}, \dots, \Gamma_K^{\mathbf{Y}}\}$ and $\mathcal{R}_{\mathbf{X}} \equiv \{\Gamma_1^{\mathbf{X}}, \dots, \Gamma_K^{\mathbf{X}}\}$ respectively. In total, there are $K = M$ elements in $\mathcal{R}_{\mathbf{Y}}$ and $\mathcal{R}_{\mathbf{X}}$ each. The number of elements in the metasets is picked as a proportion $\rho_{\mathbf{Y}}$ and $\rho_{\mathbf{X}}$ of the total number of points in \mathbf{Y} and \mathbf{X} respectively. Variation in the values of the proportion factors decides the magnitude of overlaps between the adjacent zones. $\rho_{\mathbf{Y}}$ and $\rho_{\mathbf{X}}$ can be different depending on the dissimilarity factors of input point sets (*e.g.*, densities and noise ratios). It is possible to set $\rho_{\mathbf{X}} = \rho_{\mathbf{Y}} = \rho$ when the densities or the number of points are roughly same for \mathbf{X} and \mathbf{Y} respectively. We choose $\rho_{\mathbf{X}}$ and $\rho_{\mathbf{Y}}$ as a function of N and M respectively and typically $\rho \in [0.02, 0.1]$. Hence, $P = \lfloor \rho M \rfloor$ (or $\lfloor \rho_{\mathbf{X}} N \rfloor$ and $\lfloor \rho_{\mathbf{Y}} M \rfloor$) nearest neighbors define each subset of the regions.

Locally multiply-linked N -body problem is solved on the multi-sets of corresponding regions. The particle-particle interactions are restricted between the regions — the goal is to refine local transformation rather than to recover a single global transformation. Henceforth, local rigid transformation tuple $\mathbf{T}_k = \{\mathbf{R}_k, \mathbf{s}_k, \mathbf{t}_k\}$ for every region $\Gamma_k^{\mathbf{Y}}$ is estimated with rotation \mathbf{R}_k , scale \mathbf{s}_k and translation \mathbf{t}_k (\mathbf{T}_k has 7 DoF). The force exerted by $\Gamma_k^{\mathbf{X}}$ on \mathbf{Y}_p is:

$$\mathbf{F}_{p \in \Gamma_k^{\mathbf{Y}}}^a = -Gm_p \sum_{q \in \Gamma_k^{\mathbf{X}}} \frac{m_q \left(\mathbf{r}_p \left(1 - \frac{\kappa_q \mathbf{r}_{pq}^2}{2} \right) - \mathbf{r}_q \right)}{(\|\mathbf{r}_p - \mathbf{r}_q\|^2 + \epsilon^2)^{\frac{3}{2}} \left(1 - \frac{\kappa_q \mathbf{r}_{pq}^2}{4} \right)^{\frac{3}{2}}}, \quad (7)$$

where $p \in \Gamma_k^{\mathbf{Y}}$. The notations in Eq. (7) are akin to the notations used in Eq. (4), *i.e.*, \mathbf{r}_p and \mathbf{r}_q (m_p and m_q) are coordinates (masses) of the points from the template and reference respectively; $r_{pq} = \|\mathbf{r}_p - \mathbf{r}_q\|$, and κ_q stands for the Gaussian curvature of X_q . We apply a coarse-to-fine policy for softening radius parameter ϵ which results in a sharp directional displacement towards true correspondences, as it falls exponentially in every iteration step t :

$$\epsilon(t) = \epsilon \exp \left(1 - \frac{t}{\xi} \right), \quad (8)$$

where $\xi \leq 150$ is the maximum number of iterations.

In every pairwise gravitational interaction, we stack the forces exerted to the points $p \in \Gamma_k^{\mathbf{Y}}$ into a force matrix \mathcal{F}_k :

$$\mathcal{F}_k^t = [\dots, \mathbf{F}_p^a - \eta v_p^t, \dots]^T, \quad (9)$$

and point velocities in the region:

$$\mathcal{V}_k^t = [\dots, v_p^t, \dots]. \quad (10)$$

Next, we obtain the unconstrained velocity updates:

$$\mathcal{V}_k^{t+1} = \mathcal{V}_k^t + \Delta t \mathcal{F}_k^t \circ [\dots, m_p^{-1}, \dots]^T, \quad (11)$$

where \circ denotes elementwise matrix multiplication, and an unconstrained updates for the displacements:

$$\mathcal{D}_k^{t+1} = \Delta t \mathcal{V}_k^{t+1}. \quad (12)$$

Taking the current coordinates of P points $(\mathbf{Y}_p)^t$ and the new unconstrained updates of the state space as $(\mathbf{Y}_p)^t + \mathcal{D}_k^{t+1}$, $\forall p \in \Gamma_k^{\mathbf{Y}}$, we first resolve \mathbf{s}_k as a curl-free component of the displacement field \mathcal{D}_k^{t+1} [15], then the absolute orientation problem [21, 18] is solved to obtain \mathbf{R}_k , and, finally, the \mathbf{t}_k is obtained as the mean of \mathcal{D}_k^{t+1} . We serially estimate \mathbf{T}_k for all $k \in \{1, \dots, K\}$ regions and forward them to the CCM step (Sec. 4.3) for the final position updates. Besides, only the velocity of the main representative point per region is updated.

4.3. Coherent Collective Motion

In Sec. 4.2, we have shown how locally multiply-linked N -body problem is solved separately for individual overlapping regions. \mathbf{Y}_i can appear in several regions. Consider a set $\Psi_i = \{\forall k : \mathbf{Y}_i \in \Gamma_k^{\mathbf{Y}}\}$. We say (i, Ψ_i) a mapping between a point index and its shared region indices (*e.g.*, the Fig. 2 illustrates that i^{th} point is shared by three regions: $\Gamma_i^{\mathbf{Y}}$, $\Gamma_{i-1}^{\mathbf{Y}}$ and $\Gamma_{i+1}^{\mathbf{Y}}$). The CCM operator Ξ is defined for (i, Ψ_i) and it regularizes the velocity v_i^t of \mathbf{Y}_i :

$$\Xi(v_i^t) = |v_i^t|(\vartheta) \left(\sum_{k \in \Psi_i} v_k^t \right), \quad (13)$$

where $(\vartheta)(.)$ is the normalization operator. Ξ preserves the velocity magnitude of the representative point \mathbf{Y}_i and replaces its direction by the mean of normalized force directions of all \mathbf{Y}_k , $\forall k \in \Psi_i$ from its shared groups. The CCM operator ensures the point trajectories do not cross over and relative point positions are preserved. Originally, the Ξ operator was proposed by Vicsek et al. [37] in the context of interactions encountered in biological systems. Similarly, we apply Ξ operator to the transformation tuple \mathbf{T}_i :

$$\Xi(\mathbf{T}_i) = \left\{ (\vartheta) \left(\sum_{k \in \Psi_i} \mathbf{R}_k \right), (\vartheta) \left(\sum_{k \in \Psi_i} \mathbf{t}_k \right), (\vartheta) \left(\sum_{k \in \Psi_i} \mathbf{s}_k \right) \right\}, \quad (14)$$

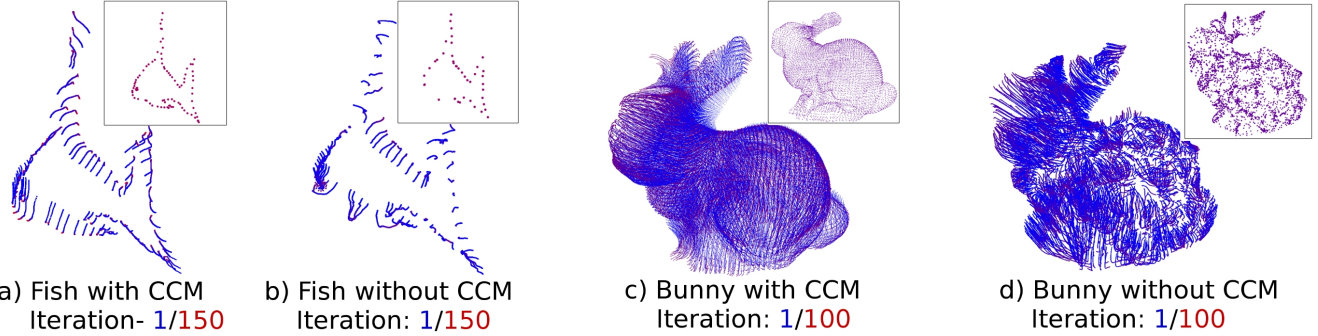


Figure 3. Point trajectories of *fish* and *bunny* datasets regularized by the proposed CCM – (a) and (c). The same trajectories collapse or cross over each other in absence of CCM regularizer – (b) and (d). These trajectories are complete path integrals of the particles leading from the initial misalignment (blue) to the registration result (red). Each superscripted figure is the registered *template*.

i.e., in every iteration, the final position is obtained by applying the $\Xi(\mathbf{T}_i)$ on \mathbf{Y}_i^t . For a given point, this consensus filter averages out several transformation tuples. The nature of collective particle dynamics in NRGA is similar to the *smoothed particle hydrodynamics* [25]. Fig. 3 shows the impact of the CCM regularizer on point trajectories.

4.4. Algorithm and Complexity Analysis

NRGA is summarized in Alg. 1. A breeze over Alg. 1 allows estimation of the NRGA complexity:

$$\mathcal{O}(\underbrace{\xi}_{\text{iterations}} \underbrace{(M \log M)}_{\text{k-d tree}} + \underbrace{M \rho M \rho N}_{\text{NRGA: N-body}} + \underbrace{M}_{\text{NRGA: CCM}}) = \mathcal{O}(M^2 N). \quad (15)$$

The coarse analysis is not taking into account that usually $\rho \in [0.02; 0.1]$. Suppose $\rho = 0.05$ and $M \leq 5 \cdot 10^4$. In this case, $\rho^2 M^2 \leq M^{1.45}$. Thus, the revised complexity will be at most $\mathcal{O}(M^\beta N)$, with $\beta = 1.45$. With smaller M , β will drop. The core implementation of NRGA requires only several hundred lines of an unoptimized C++ code.

5. Evaluation

We perform experiments on a platform with 32 GB RAM and Intel i7-6700K CPU running at 4.0GHz. We typically set $\eta = 0.05$, $G = 1.67$, $\rho = 0.05$, $\Delta t = 0.006$, $\xi = 100$ and $\epsilon = 0.1$. All other methods [1, 5, 26] are running entirely in Matlab, except GMMReg [20] which calls a Linux executable compiled from a C++ source.

Evaluation methodology and datasets. A thorough quantitative evaluation is performed on synthetic benchmark datasets *fish*, *line* (2D) and *bunny* (3D) with known ground truth correspondences. The input template data is modified in four degradation scenarios and 100 experiments are run for each of the scenarios. We report the root-mean-squared error (RMSE) value on every run defined as:

$$E_{rmse} = \sqrt{\frac{1}{N} \sum_{j=1}^N (r_{ij} - E_{mean})^2}, \quad (16)$$

Algorithm 1: Non-Rigid Gravitational Approach

Input: a reference $\mathbf{X}_{N \times D}$ and a template $\mathbf{Y}_{M \times D}$
Output: a displacement field $\mathcal{T}(\mathbf{Y}, \mathbf{T})$ registering \mathbf{Y} to \mathbf{X}
Parameters : $\epsilon \in (0, 1]$, $\eta \in (0, 1]$, G , $m(Y)$, $m(X)$, Δt , $\rho \in [0.02, 0.1]$, $\epsilon_E = 10^{-4}$, ξ

```

1 Initialization:  $\mathbf{T} = \mathbf{0}$ 
2 build a k-d tree on  $\mathbf{X}$ 
3 while  $|\phi_g^{curr} - \phi_g^{prev}| < \epsilon_E$  or  $t \leq \xi$  do
4   build a k-d tree on  $(\mathbf{Y})^t$ 
5   build multi-set of regions  $\mathcal{R}_X$  (Sec. 4.2)
6   build multi-set of regions  $\mathcal{R}_Y$  (Sec. 4.2)
7   for all  $k \in \{1, \dots, M\}$  do
8     select the regions  $\Gamma_k^Y$  and  $\Gamma_k^X$  from  $\mathcal{R}_Y$  and  $\mathcal{R}_X$ 
9     compute  $\mathcal{F}_k^t$  using Eqs. (6) – (9)
10    compute  $\mathcal{V}_k^{t+1}$  and  $\mathcal{D}_k^{t+1}$  using Eqs. (11) – (12)
11    compute  $\mathbf{T}_k = \{\mathbf{R}_k, \mathbf{s}_k, \mathbf{t}_k\}$  for  $\Gamma_k^Y$ :
12      ▷ solve for  $\mathbf{s}_k$  from the curl-free component of  $\mathcal{D}_k^{t+1}$  [15]
13      ▷ solve absolute orientation problem for  $\mathbf{R}_k$  [21, 18]
14      ▷  $\mathbf{t}_k = \text{mean}(\mathcal{D}_k^{t+1})$ 
15    for all  $\mathbf{Y}_k$ ,  $k \in \{1, \dots, M\}$  do
16      update velocities  $v_k^{t+1} = \Xi(v_k^{t+1})$  using Eq. (13)
17      update transformation  $\mathbf{T}_k^{t+1} = \Xi(\mathbf{T}_k^{t+1})$  using Eq. (14)
18    update  $\mathbf{Y}^{t+1} = \mathcal{T}(\mathbf{Y}^t, \mathbf{T})$ 

```

where E_{mean} denotes mean error. *First*, we introduce uniformly and Gaussian distributed noise into the templates, in the amounts ranging from 5% to 60% of the total points, in every run of the experiment. Additional input noises increase the number of uncertain correspondences and make the problem more ill-posed. *Second*, we randomly perturb the initial point positions in template. The direction and magnitude of perturbation are obtained as the realizations of a Gaussian distribution. The magnitude of perturbation increases linearly with every experimental attempt. *Third*, we randomly delete 20% of the original data in a chunk from the *templates*. The *fourth* scenario is imposing random misalignment on the template where the axis-angle orientation values ($\theta_x, \theta_y, \theta_z$) are the realizations from a uniform dis-

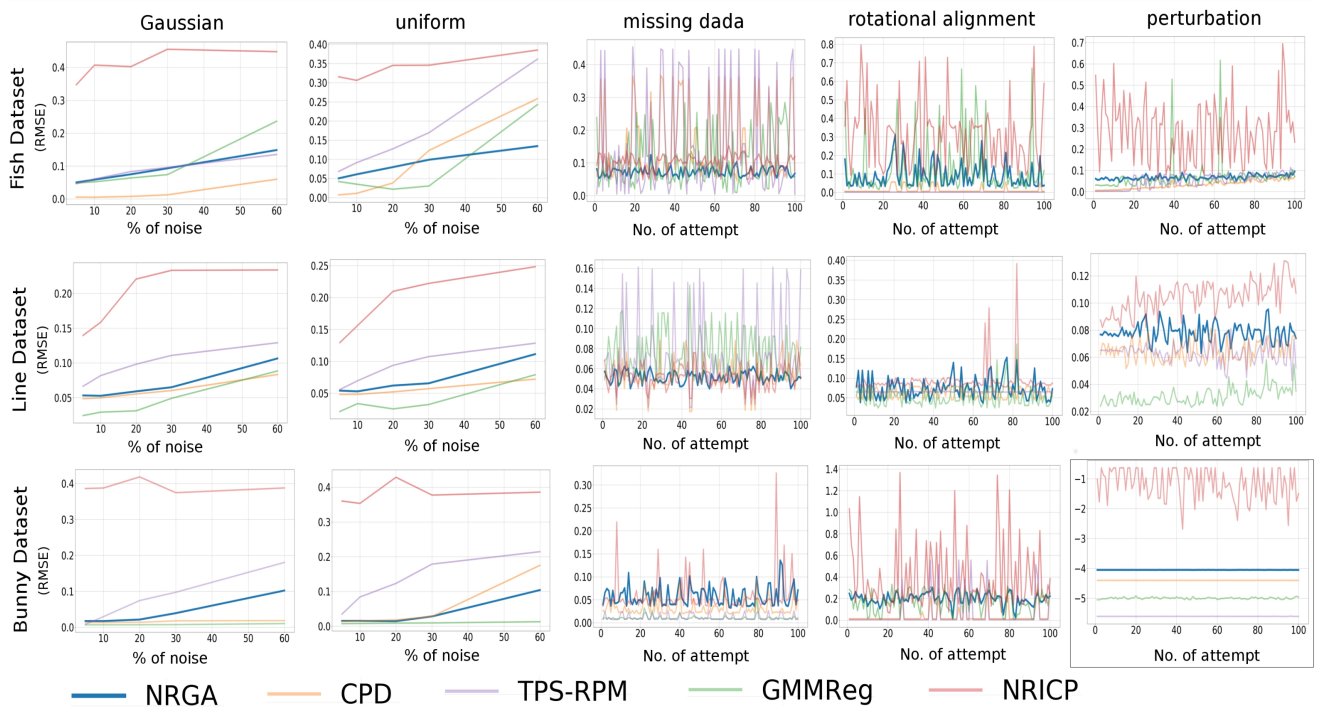


Figure 4. Quantitative results on *fish*, *line*, and *bunny* (in 1st, 2nd, and 3rd row respectively) show the error statistics for the cases with Gaussian noise, uniform noise, missing data patterns, rotations and perturbed setting (ordered in columns). NRGA is the most stable method under uniform noise and missing data, with lowest RMSE. The high peaks of GMMReg [20] and NRICP [1] are due to inherent instability. The bottom right graph shows $\log_e(E_{rmse})$ values for clear perception.

tribution $\mathcal{U}(-\frac{\pi}{4}, \frac{\pi}{4})$. Although, in non-rigid registration an optimal rigid pre-alignment is considerable, we show that NRGA can still cope with fairly misaligned point sets.

Compared methods. We compare several widely-used and state-of-the-art methods for non-rigid point set registration, *i.e.*, non-rigid ICP [1], TPS-RPM [5], CPD [26] and GMMReg [20]. We choose optimal settings for every method — this allows us to compare the best possible performances in the corresponding scenarios.

Results. Quantitative results shown in Fig. 4 reveal NRGA’s strength against uniform noise — with increasing noise, the relative accuracy of NRGA increases (for the case of 60% of noise, NRGA shows the lowest RMSE on two datasets). For the Gaussian noise, the winner is CPD — this approach explicitly models Gaussian noise, and we were always choosing the respective optimal parameter. Nevertheless, NRGA is close to GMMReg and TPS-RPM which do not make such assumption. NR-ICP fails on the experiments with noise. In the case of missing data, NRGA significantly outperforms all compared methods with consistent performance. NRGA shows stability as the error does not fluctuate across all different scenarios and datasets.

In Fig. 5, selected results from the experiments with missing data are shown. Note how NR-ICP, TPS-RPM

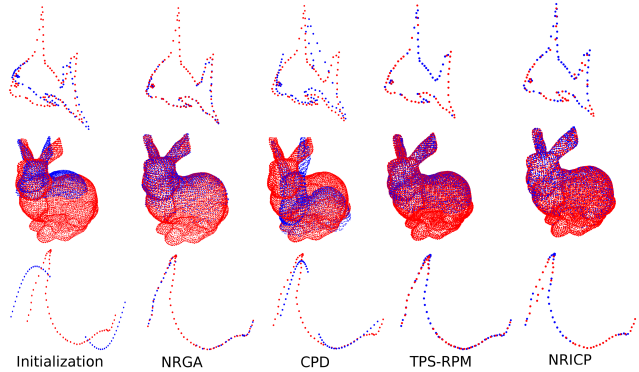


Figure 5. NRGA outperforms other evaluated methods in the handling of missing data. In this picture, results of evaluated methods on *fish*, *bunny* and *line* datasets are shown. In this experiment, more than 30% of points have been removed from all templates.

and CPD either stretch or dilate the template. In contrast, NRGA displaces points towards the appropriate regions as the attractive force function is parameterized by shape curvature. In Fig. 1, we demonstrate the performance of NRGA on real data (image registration). 2D point sets originate from computer tomography (CT) of a human brain [38]. Both images represent the same state and differ only by a

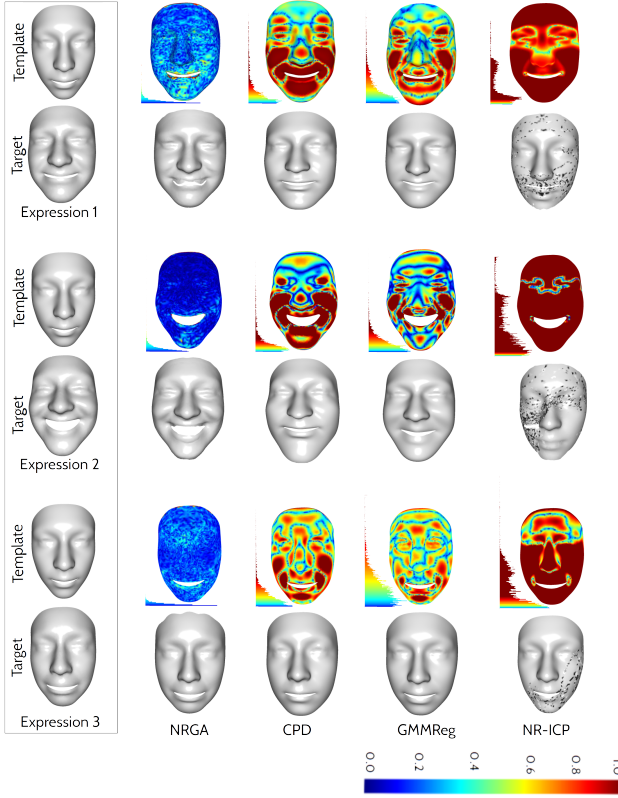


Figure 6. Qualitative results of non-rigid point set registration methods: NRGA, CPD [26], GMMReg [20], NR-ICP [1] when applied to human faces (from [4] on BU-3DFE [41]) differ in their expressions and spatial scaling. The upper and lower row in all pairs illustrate the Hausdorff distance between the target and the deformed template as a color-map (with histogram).

rectification applied on the reference image. 2D point sets are obtained by the sampling of image contours.

Regarding the practical applications of NRGA, qualitative registration results on human faces (BU-3DFE datasets [41]) using different methods are shown in Fig. 6. The *template* and *target* faces differ by facial expression and scaling factor. NRGA achieved high correspondence accuracy and geometric consistency because of using the locally aware global topology preserving CCM operator. Probabilistic approaches overfit ignoring the local minimas, whereas nearest neighbor approach is not aware of the intrinsic geometry. The noticeable point is that NRGA uses only positions and does not use other geometric attributes (*e.g.*, face or vertex normals).

We also evaluate the performance of NRGA on the real scan data. Two types of face scans are captured to test NRGA – 1) The frontal face as a part of our full body scan using multi-view system [16]. We tag this scan as the *reference*. The *template* is a synthetic data with no facial details. The scan and template contain $\simeq 3.9K$ and $4K$

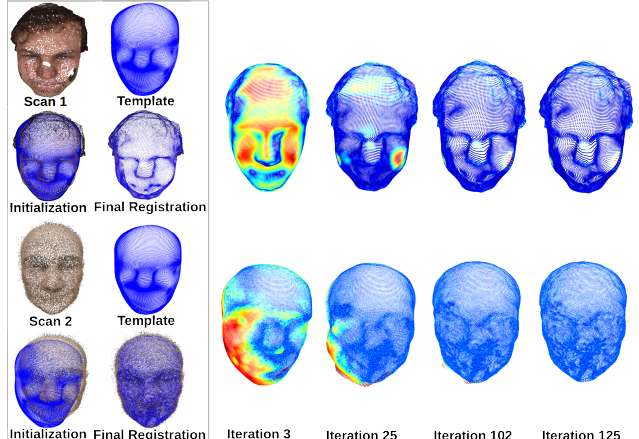


Figure 7. 1st experimental instance: in the *first two rows*, a synthetic *template* with no geometric level of details is registered to a scan data (point sets only) with holes and complex surface details like hair and skin roughness. 2nd experimental instance: in the *last two rows*, the *template* is same as 1st, the scan contains significant low-amplitude noise and little geometric details of the underlying surface. In both cases, NRGA robustly registers *template* to *scans*. Iterative results at the *right* side show distance error with same color coding as in Fig. 6.

points respectively. The *reference* face contains complex details on the surface (*e.g.*, curly hair, rough skin membranes, and several missing chunks). 2) The second scan is a point cloud with significant amount of low-amplitude noises. Fig. 7 shows that NRGA accurately fits the template onto real scans in these challenging scenarios.

6. Conclusions and Future Directions

In this draft, we have presented NRGA — the first physics-based algorithm for non-rigid point set registration of gravitational class. NRGA interprets alignment problem as a series of altered relativistic N -body problems in a space with constant Gaussian curvature. The curvature of the reference operates as a local inherent shape descriptor and influences gravitational attraction. The core CCM regularization merges multiple update proposals for the same point from several overlapping regions. Thorough experiments have shown either state-of-the-art or superior robustness of NRGA in scenarios with noisy and missing data. At the same time, real data examples demonstrated the maturity of our approach for practical applications (*e.g.*, medical image registration and template to scan fitting of faces).

Acknowledgements

This work was partially supported by the project DYNAMICS (01IW15003) of the German Federal Ministry of Education and Research (BMBF). We thank Sony Technology Center Stuttgart (Sony EuTEC) for collaborating and sharing scan dataset.

References

- [1] B. Amberg, S. Romdhani, and T. Vetter. Optimal step non-rigid icp algorithms for surface registration. In *Computer Vision and Pattern Recognition (CVPR)*, 2007. 1, 3, 6, 7, 8
- [2] P. J. Besl and N. D. McKay. A method for registration of 3-d shapes. *Transactions on Pattern Analysis and Machine Intelligence (TPAMI)*, 14(2):239 – 256, 1992. 1, 2
- [3] F. Bonarrigo, A. Signoroni, and M. Botsch. Deformable registration using patch-wise shape matching. *Graphical Models*, 76(5):554–565, 2014. 1
- [4] A. Brunton, A. Salazar, T. Bolkart, and S. Wuhrer. Review of statistical shape spaces for 3d data with comparative analysis for human faces. *Computer Vision and Image Understanding (CVIU)*, 128:1–17, 2014. 2, 8
- [5] H. Chui and A. Rangarajan. A feature registration framework using mixture models. In *Mathematical Methods in Biomedical Image Analysis*, pages 190–197, 2000. 6, 7
- [6] H. Chui and A. Rangarajan. A new point matching algorithm for non-rigid registration. *Computer Vision and Image Understanding (CVIU)*, 89(2-3):114–141, 2003. 2, 3
- [7] W. Deng, H. Zou, F. Guo, L. Lei, S. Zhou, and T. Luo. A robust non-rigid point set registration method based on inhomogeneous gaussian mixture models. *The Visual Computer*, 2017. 1
- [8] Y. Deng, A. Rangarajan, S. Eisenschenk, Vemuri, and C. Baba. A riemannian framework for matching point clouds represented by the schrödinger distance transform. In *Computer Vision and Pattern Recognition (CVPR)*, 2014. 1, 2, 3
- [9] F. Diacu. The solution of the n-body problem. *The Mathematical Intelligencer*, 18(3):6670, 1996. 3
- [10] F. Diacu. The classical n-body problem in the context of curved space. *Canadian Journal of Mathematics*, 69:790–806, 2017. 2, 4
- [11] A. Einstein. Die grundlage der allgemeinen relativitätstheorie. *Annalen der Physik*, 354(7):769 – 822, 1916. 3
- [12] B. Fischer and J. Modersitzki. Curvature based image registration. *Journal of Mathematical Imaging and Vision*, 18(1):81–85, 2003. 1, 3
- [13] R. Gal and D. Cohen-Or. Salient geometric features for partial shape matching and similarity. *ACM Transactions on Graphics*, 25(1):130–150, 2006. 3
- [14] S. Ge and G. Fan. Non-rigid articulated point set registration with local structure preservation. In *Computer Vision and Pattern Recognition Workshops (CVPRW)*, pages 126–133, 2015. 3
- [15] V. Golyanik, S. A. Ali, and D. Stricker. Gravitational approach for point set registration. In *Computer Vision and Pattern Recognition (CVPR)*, 2016. 1, 2, 3, 5, 6
- [16] V. Golyanik, G. Reis, B. Taetz, and D. Stricker. A framework for an accurate point cloud based registration of full 3d human body scans. In *2017 Fifteenth IAPR International Conference on Machine Vision Applications (MVA)*, 2017. 8
- [17] M. Greenspan and G. Godin. A nearest neighbor method for efficient icp. In *International Conference on 3-D Digital Imaging and Modeling (3DIM)*, pages 161–168, 2001. 2
- [18] B. K. P. Horn. Closed-form solution of absolute orientation using unit quaternions. *Journal of the Optical Society of America A*, 4(4):629–642, 1987. 5, 6
- [19] E. Ilg, N. Mayer, T. Saikia, M. Keuper, A. Dosovitskiy, and T. Brox. Flownet 2.0: Evolution of optical flow estimation with deep networks. In *Computer Vision and Pattern Recognition (CVPR)*, 2017. 1
- [20] B. Jian and B. C. Vemuri. A robust algorithm for point set registration using mixture of gaussians. In *International Conference for Computer Vision (ICCV)*, pages 1246 – 1251, 2005. 1, 2, 6, 7, 8
- [21] W. Kabsch. A solution for the best rotation to relate two sets of vectors. *Acta Crystallographica Section A*, 32(5):922 – 923, 1976. 4, 5, 6
- [22] K. G. M. Sethi, A. Rangarajan. The schrödinger distance transform (sdt) for point-sets and curves. In *Computer Vision and Pattern Recognition (CVPR)*, 2012. 2
- [23] J. Ma, J. Zhao, J. Jiang, and H. Zhou. Non-rigid point set registration with robust transformation estimation under manifold regularization. In *Conference on Artificial Intelligence (AAAI)*, pages 4218–4224, 2017. 2
- [24] J. Ma, J. Zhao, and A. L. Yuille. Non-rigid point set registration by preserving global and local structures. *IEEE Transactions on Image Processing*, 25(1):53–64, Jan 2016. 3
- [25] J. J. Monaghan. Smoothed particle hydrodynamics. *Annual Review of Astronomy and Astrophysics*, 30(1):543 – 574, 1992. 6
- [26] A. Myronenko and X. Song. Point-set registration: Coherent point drift. *Transactions on Pattern Analysis and Machine Intelligence (TPAMI)*, 2010. 1, 3, 6, 7, 8
- [27] V. Nityananda and J. C. A. Read. Stereopsis in animals: evolution, function and mechanisms. *Journal of Experimental Biology (JEB)*, 220(14):2502–2512, 2017. 3
- [28] X. Q. P. Yang. Direct computing of surface curvatures for point-set surfaces. In *Eurographics Symposium on Point-Based Graphics (SPBG)*, 2007. 4
- [29] C. Papazov and D. Burschka. Deformable 3d shape registration based on local similarity transforms. *Computer Graphics Forum (CGF)*, 30(5):1493–1502. 1
- [30] S. Rusinkiewicz and M. Levoy. Efficient variants of the ICP algorithm. In *International Conference on 3-D Digital Imaging and Modeling (3DIM)*, 2001. 2
- [31] L. G. Sanchez Giraldo, E. Hasanbelliu, M. Rao, and J. C. Principe. Group-wise point-set registration based on Renyi’s second order entropy. In *Computer Vision and Pattern Recognition (CVPR)*, 2017. 3
- [32] J. Sun, M. Ovsjanikov, and L. Guibas. A concise and provably informative multi-scale signature based on heat diffusion. In *Symposium on Geometry Processing (SGP)*, pages 1383–1392, 2009. 3
- [33] G. K. L. Tam, Z. quan Cheng, Y. kun Lai, F. C. Langbein, Y. Liu, D. Marshall, R. R. Martin, X. fang Sun, and P. L. Rosin. Registration of 3d point clouds and meshes: A survey from rigid to nonrigid. *Transactions on Visualization and Computer Graphics (TVCG)*, 19(7):1199 – 1217, 2013. 1, 3
- [34] A. Tevs, M. Bokeloh, M. Wand, A. Schilling, and H. P. Seidel. Isometric registration of ambiguous and partial data.

- In *Computer Vision and Pattern Recognition (CVPR)*, pages 1185–1192, 2009. 3
- [35] The Stanford 3D Scanning Repository. <http://graphics.stanford.edu/data/3Dscanrep/>. 2
- [36] O. van Kaick, H. Zhang, G. Hamarneh, and D. Cohen-Or. A survey on shape correspondence. *Computer Graphics Forum (CGF)*, 30(6):1681 –1 707, 2011. 1
- [37] T. Vicsek, A. Czirók, E. Ben-Jacob, I. Cohen, and O. Shochet. Novel type of phase transition in a system of self-driven particles. *Physical Review Letters (PRL)*, 75:1226–1229, 1995. 2, 5
- [38] D. Škerl, B. Likar, J. M. Fitzpatrick, and F. Pernuš. Comparative evaluation of similarity measures for the rigid registration of multi-modal head images. *Physics in Medicine and Biology*, 52(18), 2007. 2, 7
- [39] G. Wang, Z. Wang, Y. Chen, X. Liu, Y. Ren, and L. Peng. Learning coherent vector fields for robust point matching under manifold regularization. *Neurocomputing*, 216:393 – 401, 2016. 3
- [40] C. M. Will. *Gravity: Newtonian, Post-Newtonian, and General Relativistic*, pages 9 – 72. Springer International Publishing, 2016. 3
- [41] L. Yin, X. Wei, Y. Sun, J. Wang, and M. J. Rosato. A 3d facial expression database for facial behavior research. In *7th International Conference on Automatic Face and Gesture Recognition (FG2006)*, pages 211–216, 2006. 2, 8
- [42] Z. Zhou, J. Zheng, Y. Dai, Z. Zhou, and S. Chen. Robust non-rigid point set registration using student's-t mixture model. *Public Library of Science (PLOS ONE)*, 9:1–11, 2014. 3